3D Finite Element Analysis of Sub-Level Caving Plan for Indicative Ground Support Requirements at Bozymchak Mine, Kyrgyzstan

Neil Bar[1], D. Smagulov[2], M. Tashtanov[2], F. Zhumadylov[2] and A. McQuillan[3]

[1] Gecko Geotechnics, Kingstown, Saint Vincent and the Grenadines
[2] KAZ Minerals, Bishkek, Kyrgyzstan
[3] Rocscience Inc, Phuket, Thailand
neil@geckogeotech.com

Abstract. Bozymchak is a copper mine in Kyrgyzstan that is transitioning from open pit to underground mining using sub-level caving method (SLC). Longitudinal SLC mining is planned to continue downward from the base of the existing open pit until mine closure. Several geotechnical investigations were completed to understand ground conditions in the deeper areas of the deposit. These included diamond core drilling, mapping of capital developments and the modelling of major geological structures. Three-dimensional (3D) stress-strain analysis was completed using the finite element method (FEM) to identify areas of risk forming from high stresses in response to SLC extraction. This paper briefly describes the stress-strain modelling, risks identified with the SLC sequence, and planned control measures to mitigate those risks.

Keywords: Finite element method, underground mining, sub-level caving.

1 Introduction

Bozymchak copper-gold mine is located in the Alu-Buka district of the Jalal-Abad region of Kyrgyzstan, 600 km south-west of Bishkek, the capital of Kyrgyzstan; and 150 km to the east of Tashkent, Uzbekistan, Figure 1.

Bozymchak mine has an average copper content of 1.12 %, gold grade of 1.96 g/t and silver grade of 13.2 g/t [1-2].

R. Hammah et al. (eds.), *Proceedings of the Rocscience International Conference 2025 (RIC 2025)*, Atlantis Highlights in Engineering 40,
https://doi.org/10.2991/978-94-6463-900-1_6

Figure 1. Bozymchak Copper-Gold Mine Location

The mine is currently transitioning from open pit to underground mining, Figure 2. Due to the challenging geotechnical conditions, it was identified that caving posed a significant risk to the stability of the existing, depleted open pit [3]. As a practical control measure to reduce the impact of this risk, pit backfilling commenced in 2023 as shown in Figure 3.

Figure 2. Bozymchak Open Pit nearing completion in 2022, looking south at granodiorite hanging wall (inter-ramp angle, IRA=63°).

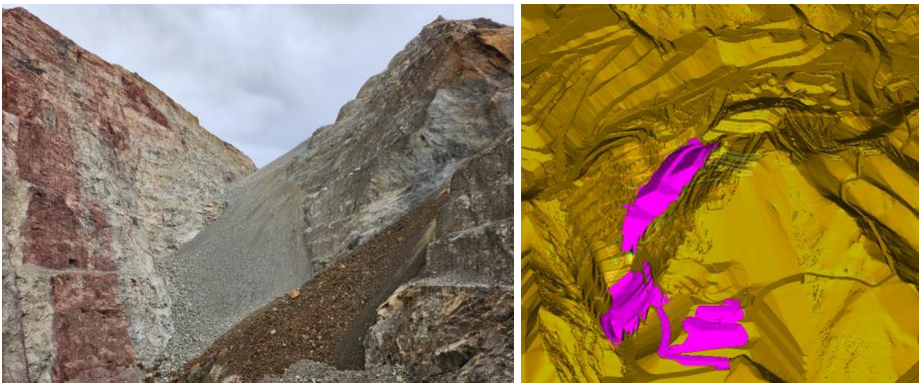

Figure 3. Left: Bozymchak pit backfilling in November 2023 looking east (limestone footwall on left). Right: Backfill design in pink.

This paper discusses the stress-strain modelling to understand risks that may develop in response to the SLC sequence, and the planned control measures to mitigate those risks.

2 Mining Context

From 2012 to 2023 the Bozymchak deposit has been partly extracted through open pit mining at a rate of 1.1M tonnes of ore per year to a depth of 300 m. Ore has been processed on site using a plant with 1.1M tonne capacity per annum. Underground mine development in preparation for SLC mining commenced in 2018 and was completed in September 2023.

Longitudinal SLC mining with an initial capacity of 300,000 tonnes of ore per year began at elevations 2130 m and 2105 m. Based on the life-of-mine plan, SLC mining is expected to reach a production rate of 1.1M tonnes of ore per year from 2024.

The life of the underground mine is nine years with proven and probable ore reserves of 9.6M tonnes with a content of 0.73% copper, 1.14 g/t gold and 7.29 g/t silver.

Backfilling of the pit using waste rock fill, as shown in Figure 3, will progressively fill the extracted portions of the SLC with gravity.

SLC mining will utilize various types of diamond-shaped ring cross-sections depending on the sub-level drift spacing which will range from 15 to 28 m, as shown in Figure 4. The standard spacing of the sublevel drifts is 25 m with a 65° shoulder angle on the rings.

Predicted average dilution during production is 21% with an ore loss of 8%. The predicted dilution is similar to most SLC mines around the world, which range from 4 to 43% [4]. However, the predicted ore loss is considerably less than most SLC mines, which are typically 10 to 20%.

Currently, the mine is investigating options for switching from diamond-shaped rings to fan-shaped rings in order to reduce the required blast hole lengths and drift spacing for improving ore extraction.

Rings are drilled using 102 mm diameter holes with lengths of 10 to 50 m with a Sandvik DL421 top hammer long-hole drill rig. ANFO granular explosives are used for blasting.

Face drilling and supporting of mine development and drifts are carried out using Sandvik DD321 two-boom jumbos.

Mucking and haulage is carried out using Sandvik LH410 loaders and TH430 dump trucks.

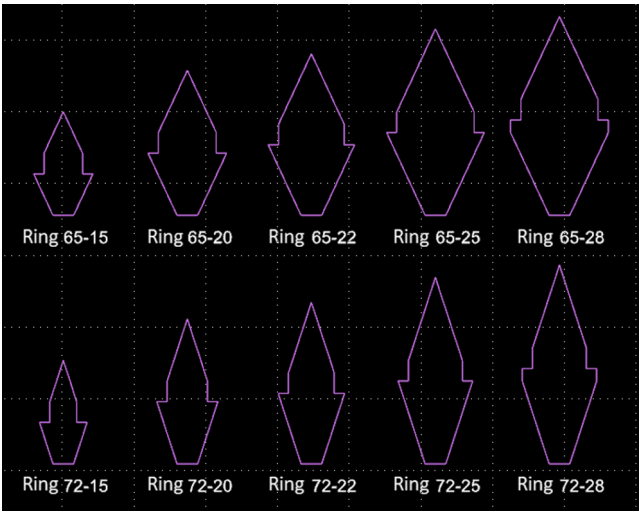

Figure 4. Design Ring Cross-Sections for SLC Mining

The mine requires approximately 3.6 to 4.0 m^3/s of fresh air per 1,000 tonnes of ore production per month, which is similar to other SLC mines.
Groundwater inflows in the lower levels of the mine are expected to range from 25 to 90 m^3 per hour depending on the season.

3 Geological Setting and Geotechnical Investigations

The Bozymchak copper-gold (Cu-Au) skarn deposit is located within in the Chatkal-Kurama region of the Tian Shan belt [5-6]. The 305 Ma skarn deposit is associated with a granodiorite porphyry intrusion as shown in Figure 5.

Sedimentary, intrusive, and metamorphic rocks form the key stratigraphic units within the Bozymchak Cu-Au deposit. Rock types comprise marbled and dolomitic limestones, skarn, serpentinite and granodiorite (from top-down; [7]):

- Limestones form the hanging wall and are very strong, coarsely bedded with minor fracturing.

- Skarns of ore bodies are timed to coincide with the contact of the granodiorite intrusion with limestone.
- Serpentinites are the weakest rocks in the deposit and alternate with skarn blocks. Serpentinite is prone to unravelling, particularly when in contact with water.
- Granodiorites form the hanging wall and are strong with discontinuous jointing.

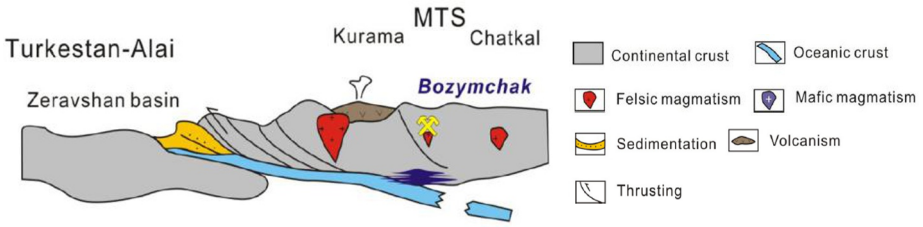

Figure 5. Tectonic settings and evolution of Chaktal-Kurama Middle Tian Shan (MTS) mountain ranges and related Cu-Au mineralization at Bozymchak [6].

Figure 6 displays a plan & cross-section of the Bozymchak deposit and planned SLC.

The Latitudinal Faults are related to the distribution of the sulphide mineralization at the deposit and have resulted in the downward displacement of part of the orebody by 200 to 280 m [8]). A complex set of steeper geological faults are present at depth, crosscutting the Latitudinal Faults and separating the orebody into various blocks.

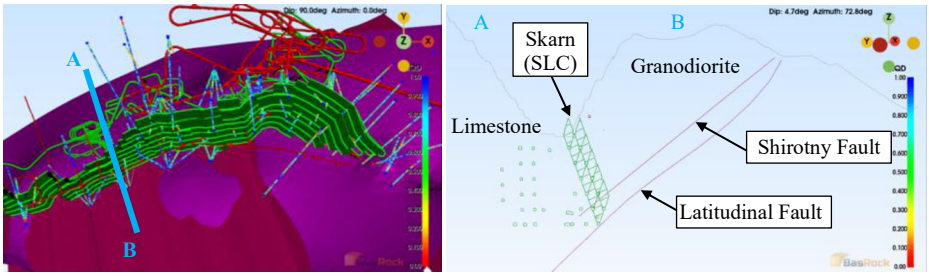

Figure 6. Left: SLC plan showing drilling data (RQD) relative to Latitudinal and Shirotny Faults. Right: Cross-section A-B of SLC plan looking east.

Several geotechnical investigations have been completed at Bozymchak to understand strength and stiffness properties of the different rock masses. Table 1 presents initial intact rock properties for the hanging wall and footwall [9].

Site investigations also included several diamond drilling campaigns to improve geological and geotechnical understanding. These included assessments of rock mass quality, RQD [10], RMR_{89} [11]; and the Q-system [12-14].

Face mapping has been used to validate and update the geotechnical model with the progression of capital developments as shown in Figure 7.

Table 1. Intact Rock Properties [9].

Rock Type	Unit Weight (kN/m^3)	UCS, σ_c (MPa)	UTS, σ_t (MPa)	Young's Modulus, E_i (GPa)	Poisson's Ratio, ν	V_p (km/s)	V_s (km/s)
Limestone (Footwall)	27	45 - 87	4 - 7	63	0.18	5.9	2.7
Granodiorite (Hanging Wall)	29	171	14	56	0.18	5.5	2.5

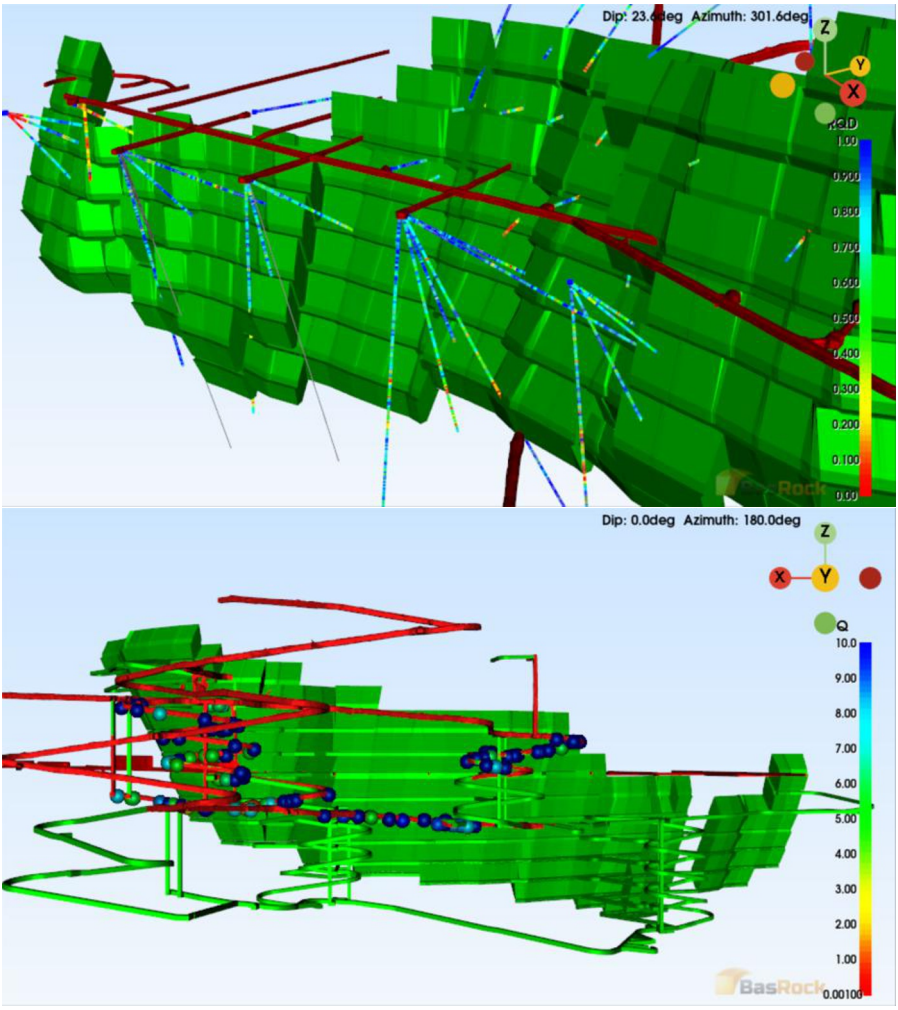

Figure 7. Geotechnical site investigations including diamond drilling into planned SLC hanging wall (top: showing RQD) and face mapping of capital developments displayed in GEM4D software by BasRock (bottom: showing Q). Note: red denotes constructed development drifts; green denotes planned developments and SLC.

Based on the Q-system and considering static, in-situ stresses (i.e. without considering mining-induced stresses), rock mass quality in the footwall and hanging wall is typically *Fair* to *Good* (Q values ranging from 4 to 20), as shown in Figure 8 for Limestone. In close proximity to the contact with the skarn orebody and near geological faults, rock mass quality can be *Very Poor* to *Poor* (Q≈1.0), Figure 9.

Figure 8. Left: Limestone Q ≈ 4 with some overbreak near a SLC drawpoint. Right: Limestone Q ≈ 10 with overbreak (roof wedge) in capital development.

Figure 9. Example of typical rock mass quality for skarn (Q ≈ 1).

4 Geotechnical Model

The geotechnical model was developed based on the lithology (rock type) model and the available intact rock and rock mass quality data which are summarized in Table 2.

Based on face mapping data including intact rock strength estimation in the field and geological strength index (GSI) assessments, the rock mass strength and stiffness properties in Table 2 were derived using the Hoek-Brown failure criterion [15].

Regional fault zones were characterized using the Mohr-Coulomb failure criterion based on rudimentary wedge failure back-analysis from the open pit (140 m high failure) and engineering judgement: c' = 100 kPa; φ' = 25°; E_m = 0.5 GPa; ν = 0.3.

No in-situ stress measurements were completed at the site; however, it was understood that anisotropic in-situ stresses were present with the horizontal to vertical stress ratio, σ_h / σ_v, ranging from 1.5 to 2.

Table 2. Rock Mass Quality, Strength and Stiffness.

Rock Type	RQD (%)	J_n	Q *	UCS (MPa)	GSI	m_i	Young's Modulus, E_m (GPa)	Poisson's Ratio, ν
Limestone	75	3	4.000	75	71	12	11	0.3
Granodiorite	70	6	10.000	150	64	29	12	0.3
Skarn	70	6	1.000	125	60	29	10	0.3
Serpentinite	40	12	0.200	100	25	15	1	0.3

5 Stress-Strain Model

A three-dimensional (3D) stress-strain model was developed using finite element method (FEM) RS3 software by Rocscience, Inc. The model comprised the latest topographical surveys including the final pit design, 2022 lithology (geology) and major structure (fault) models and the proposed underground development and SLC design.

Model stages were used to sequence excavations. The excavation sequence was simplified as follows to reduce model computational time:

1. Stage 1: In-situ conditions at end of 2022 including all existing underground developments surface excavations (including end of pit design).
2. Stage 2: Excavation of all underground capital and mine production development
3. Stage 3: SLC Excavation between 2023 and 2025.
4. Stage 4: SLC Excavation between 2026 and 2028.
5. Stage 5: SLC Excavation between 2029 and 2031.

The stress-strain model uses a four-noded, graded tetrahedra mesh comprising almost 18 million elements with a minimum size of 3 m applied to the underground excavations.

Model assumptions included dry conditions given the topographic elevation of most of the deposit. Materials were considered to be elastic, meaning they cannot 'fail' in the model, but can be assessed using a failure envelope or Strength Factor.
Initial element loading for the models including body force due to gravity and field stresses: $\sigma_h / \sigma_v = 2$.

As shown in Figure 10, the Strength Factor on the hanging wall is less than one (i.e. shear failure) between Stages 3 to 5. That is, the hanging wall is not expected to

remain stable and should experience overbreak to a depth of approximately 50 m, which may be a considerable source of dilution if unmanaged.

In Stage 5, the Strength Factor is less than zero for the Shirotny and Latitudinal faults, indicating tensile stresses, or fault reactivation.

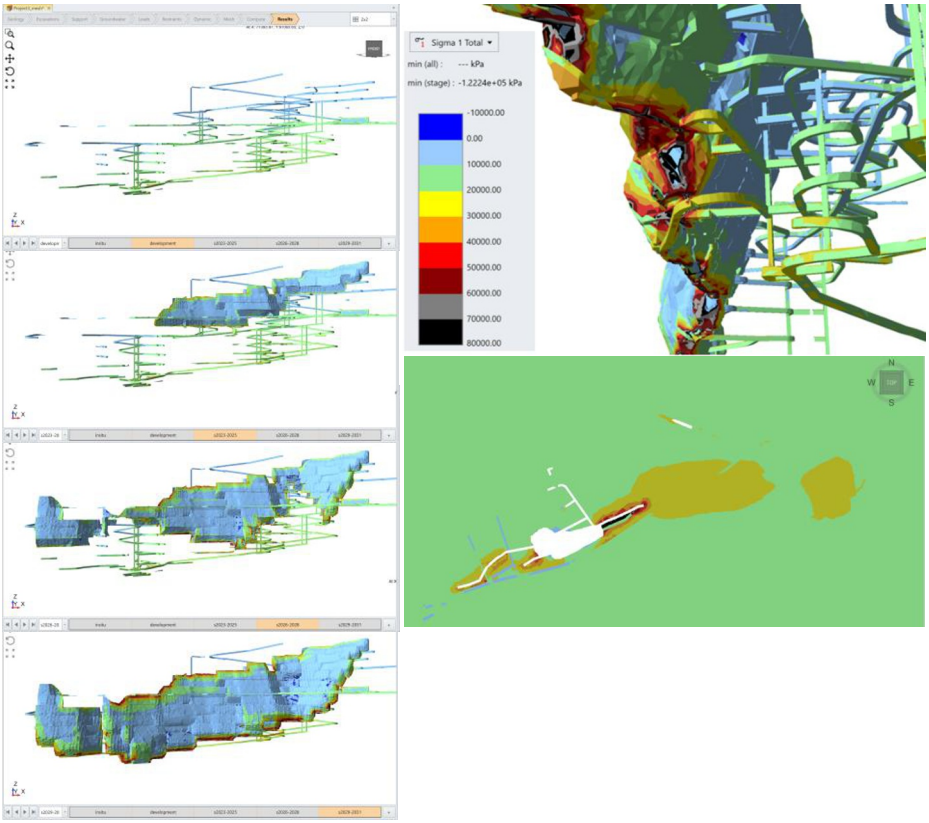

Figure 10. 3D FEM results showing Maximum Principal Stress (σ_1) acting on the underground excavations (pit not shown for clarity). Left (top to bottom): Stages 2, 3 4 & 5. Right: Maximum Principal Stress (σ_1) locally exceeding 80 MPa on 1930L near Shirotny Fault.

Stresses increase proportionally with depth and SLC excavation progress. However, high stress concentrations are evident near the Shirotny and Latitudinal faults. As shown in Figure 10, the maximum principal stress, σ_1, may locally exceed 80 MPa on 1930L and the maximum shear stress ratio frequently exceeds 0.4 in the pillar between the developments and the faults.

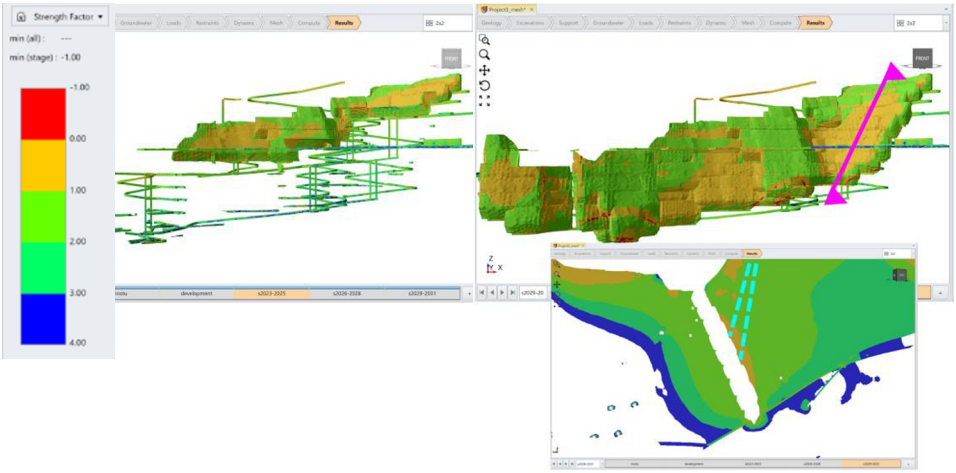

Figure 11. 3D FEM results. Left: Stage 3. Right: Stage 5. Strength Factor less than one on SLC hanging wall and less than zero in the Shirotny and Latitudinal Faults. Cross-section showing potential depth of hanging wall overbreak & proposed boreholes for monitoring.

6 Evaluation of Failure Modes

Numerical model outputs were used to assist in understanding potential modes of rock mass instability that the underground excavations may be exposed to at different locations and at various stages of mine development and production. Figure 12 originated from concepts and case studies by Hoek & Brown [16] and has been developed over 40+ years to relate in-situ stress conditions using the stress versus strength ratio and GSI (previously RMR_{76}) to indicate potential failure modes in underground excavations [17-18]. Based on Figure 12, the following ground behaviors can be expected:

- Block falls and wedge failures at low stresses to brittle failure of intact rock at intermediate and high stresses in Limestone, Granodiorite and Skarn.
- Unravelling to squeezing in Serpentinite from low to high stresses.

For openings excavated within a brittle rock mass under high stresses, the magnitudes of induced stresses are almost always high enough to initiate rock mass damage and cause failure during excavation. Typically, the worst problems develop where high levels of strain energy accumulate in the rock mass, often adjacent to active underground development or production areas. When high levels of strain energy accumulate, moderate to severe seismic events and/or rockbursts can be triggered [19]. As shown in Figure 13, rockbursts are classified into [20]:

- Strain (inherent) burst – magnitudes of in-situ stress are high enough to cause failure in the initial step of the excavation.
- Pillar (induced) burst – remaining stresses after the main excavation of rock around the pillar.
- Fault-slip burst – deformation or sliding along an existing major geological structure.

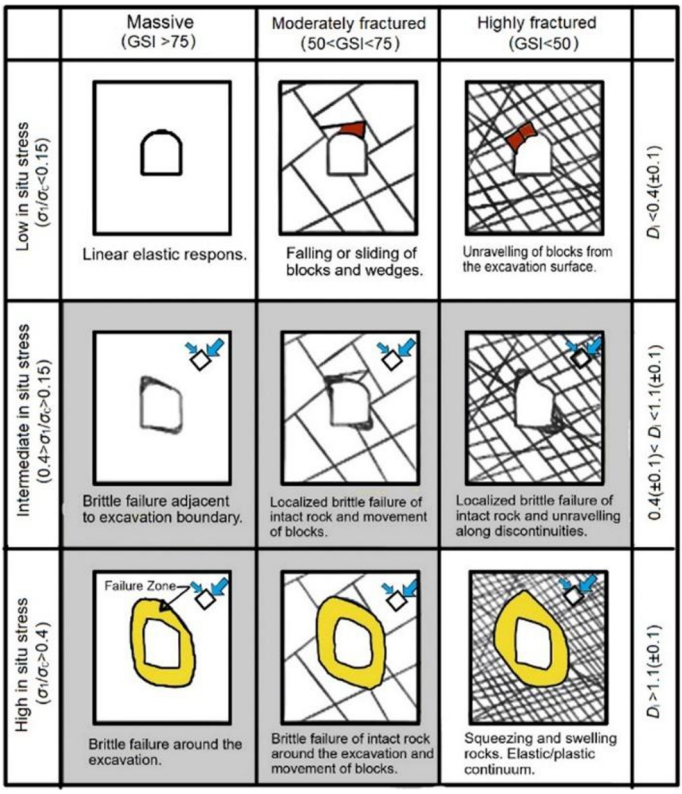

Figure 12. Potential failure modes based on the ratio of maximum in-situ stress and GSI [16-18].

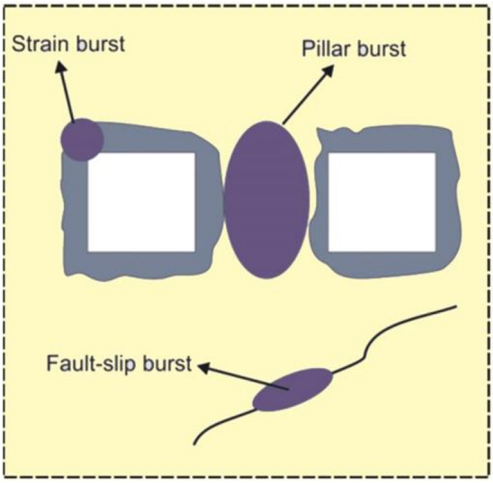

Figure 13. Schematic representation of potential rockbursts: strain burst, pillar burst and fault-slip burst [19].

Strain burst mechanisms (decreasing the radial stress and increasing the tangential stress) induce rock mass failure around the perimeter of an excavation. This often develops as spalling and slabbing failure and no damaging vibration (seismicity) occurs prior to rock failure, i.e. the damaging vibration is generated during or after bursting.

Pillar burst can occur in deep excavations in brittle rock masses when high strain energy is stored within them. Pillar burst occurs under low to moderate confinement conditions and are often related to the pillar's width to height ratio.

Fault-slip burst or shear burst occur under high confinement conditions and are triggered by underground development, underground blasting and extraction, which reactivate pre-existing faults, or form seismically active structural zones [18].

The major principal stress, σ_1, is used to illustrate high stress concentrations, which may pose a risk to development or production areas. These risks are associated with brittle failure of intact rock around the excavation and movement of blocks in moderately fractured rock masses and squeezing in highly fractured rock masses as indicated in Figure 12.

For developments in brittle rock, Stacey and Page [21] found that the ratio of σ_1 to the uniaxial compressive strength (σ_c) of the rock can be used as a simple criterion for assessing potential failure as shown in Table 3.

Table 3. Empirical stability criteria for massive brittle rock [21].

σ_1 / σ_c	Description of Condition
< 0.20	No particular problems.
0.20 – 0.40	Spalling from surface parallel to σ_1. Heavier support required.
0.40 – 0.50	Heavy support required. Major spalling.
0.50 – 0.67	Very dangerous and difficult to keep open. Support heavy and costly.
> 0.67	Impractical or extremely difficult to maintain open.

Martin et al. [17] found that as $\sigma_1 / \sigma_c > 0.33$, fracturing extends across the full span of a tunnel roof at higher stress magnitudes and that an arched roof is more favorable.

The Q-system also considers σ_1 and σ_c for describing the potential impacts of induced stresses in competent rocks as shown in Table 4.

Table 4. Rock stress problems in competent rock (forms part of SRF_b in the Q-system) [13-14].

σ_c / σ_1	σ_1 / σ_c	Description of Condition
>200	<0.005	Low stress, near surface, open joints.
200 – 10	0.005 – 0.10	Medium stress, favorable stress conditions.
10 – 5	0.10 – 0.20	High stress, very tight structure. Usually favorable to stability, may be unfavorable for wall stability.
5 – 3	0.20 – 0.33	Moderate slabbing after one hour in massive rock.
3 – 2	0.33 – 0.50	Slabbing and rockburst after a few minutes in massive rock.

Deviatoric (differential) stress is calculated by subtracting the minimum (or minor) principal stress from the maximum (or major) principal stress: $\sigma_1 - \sigma_3$.

Deviatoric stress levels have been used to evaluate strain burst severity and rock mass damage around the excavation zone as shown in Table 5 [19].

Maximum shear stress ratio is calculated by dividing the deviatoric stress by the UCS of intact rock (σ_c).

Table 5. Rock mass damage and strain burst risk based on level of deviatoric stress [19].

$(\sigma_1 - \sigma_3) / \sigma_c$	Rock Mass Damage	Likelihood of Strain Burst
0.35	No to minimum	No
0.35 - 0.45	Minimum	No
0.45 - 0.60	Moderate	Minor
0.60 - 0.70	Moderate to major	Moderate
>0.70	Major	High

Considering the empirical stability criteria by Stacey & Page [21], Figure 14 shows that $\sigma_1 / \sigma_c > 0.6$ on 1930 L, suggesting it may be difficult to maintain open with rock burst in massive rock. The maximum shear stress ratio on 1930 L locally exceeds 0.5 in proximity to the major faults (Figure 15), suggesting moderate rock mass damage with a minor likelihood of strain burst.

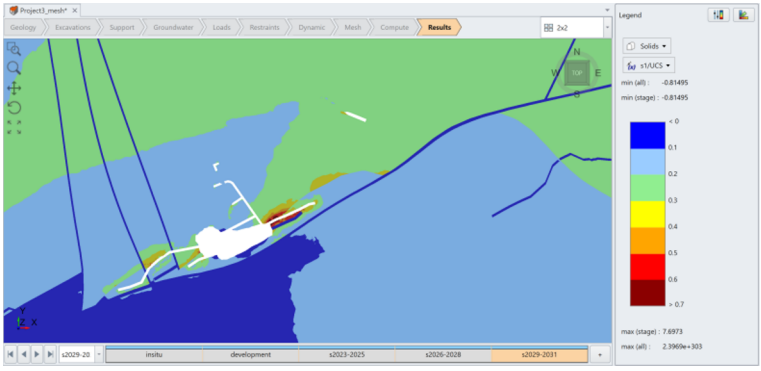

Figure 14. 3D FEM results showing σ_1 / σ_c on underground development during Stage 5. Ratio exceeding 0.6 in pillar between capital development and Shirotny fault on 1930 L.

7 Forecasting Ground Support Requirements in Response to Mining Induced Stresses

Initial studies into ground support requirements generally only consider in-situ stresses. On 1930 L, σ_1 is approximately 20 MPa. Based on the stress-strain modelling, σ_1 is expected to increase to approximately 50 MPa (typical) near development drives toward the end of SLC mining, with maximum σ_1 values locally reaching 80 MPa.

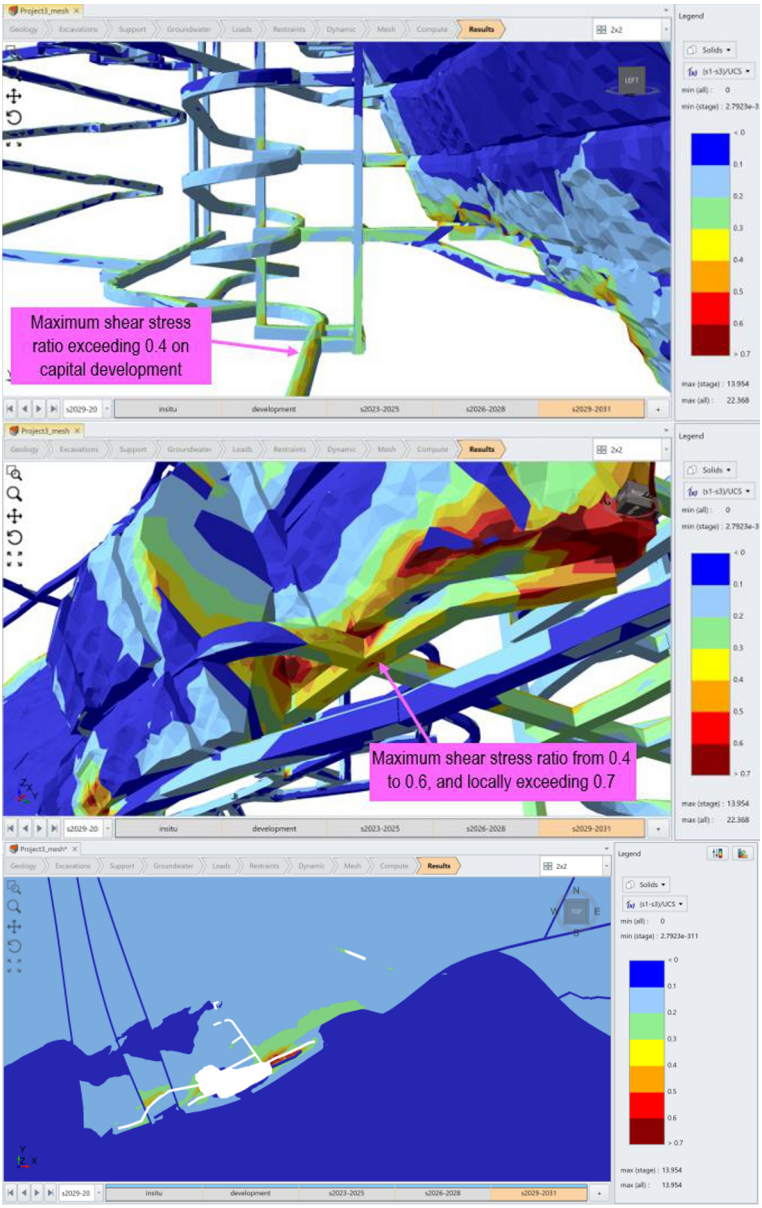

Figure 15. 3D FEM results showing Maximum Shear Stress Ratio on underground developments during Stage 5. Maximum shear stress ratio exceeding 0.4 in pillar between capital development and Shirotny fault on 1930 L.

Mining induced stresses are approximately double the in-situ stress, which is considered realistic as it has occurred in other SLC mines including Kiirunavaara mine in Sweden [22].

Such profound changes in stresses in proximity to excavations as a result of SLC mining have an impact on the stress reduction factor, SRF_b, in the Q-system.

As demonstrated in Table 6, Q values change significantly in response to mining induced stresses. That is, as SLC mining progresses, conceptual ground support requirements for different geotechnical domains will change, i.e. increase in areas subject to high mining induced stresses.

Table 6. Q value based on in-situ and mining induced stresses.

Stress State	In-Situ	Mining Induced	
		Typical	Maximum
σ_1 on 1930 L (MPa)	20	50	80
Limestone	4.000	0.333	0.250
Granodiorite	10.000	0.350	0.078
Skarn	1.000	0.023	0.010
Serpentinite	0.200	0.004	0.002

Figure 16 provides an indication of ground support requirements for pre-mining conditions and in response to mining induced stresses. It should be noted that the heavier support is only required in areas expected to experience higher stresses, i.e. not everywhere in the mine.

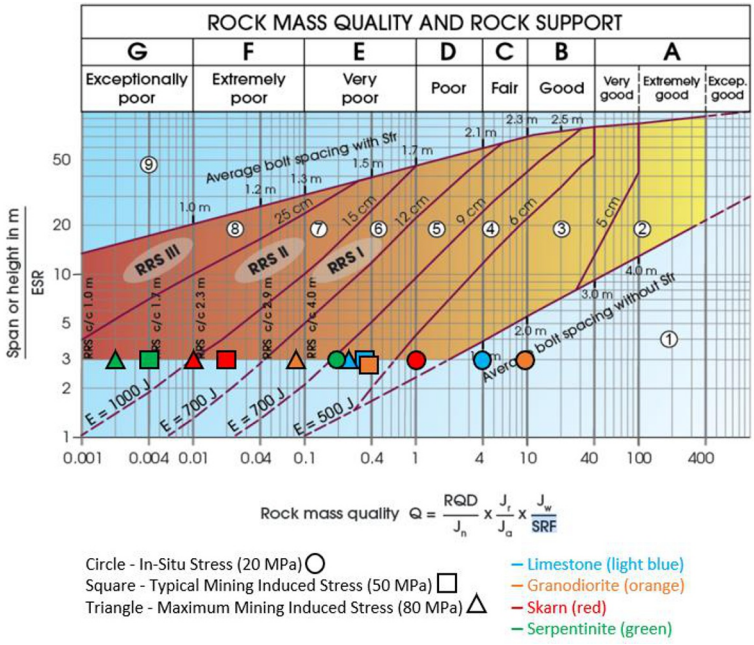

Figure 16. Rock Mass Quality (Q-system) and Rock Support Chart [23] for Different Rock masses under Different Stresses at 1930 L.

Pre-mining conditions require limited support in Limestone and Granodiorite due to relatively small spans, typically 5 m, and *Fair* rock mass quality. As shown in previous photographs, Figure 8, these excavations are generally unsupported with some spot bolting and mesh in more fractured areas (i.e. Support Category 1). However, as stresses increase in response to SLC mining, e.g. 50 MPa on 1930 L, the rock mass quality may reduce to *Very Poor* and require Support Category 4 (6-9 cm thick fibre-reinforced shotcrete and bolting).

Similar increases in support will be required in the Skarns and Serpentinites; however, these are generally less prevalent, especially in long-term developments.

8 Subsidence Zone

In preparation for caving, the bottom of the open pit has been partly backfilled using rock fill, Figure 3, to preload the breakthrough zones and to limit the size of the crater and instability of the south wall above the cave.

Modelled maximum shear strain in Figure 17 indicates shearing along the Shirotny fault reaching the surface behind the south wall of the open pit. In combination with the modelled deformation in Figure 18, the re-activation of the Shirotny and Latitudinal faults indicates the development of an extensive subsidence zone above the hanging wall. Since the models are not calibrated, these results do not provide absolute deformation magnitude predictions; rather they indicate areas most susceptible to movement. Progressive movement along these faults with SLC progression is expected to result in significant displacements on the south wall of the open pit.

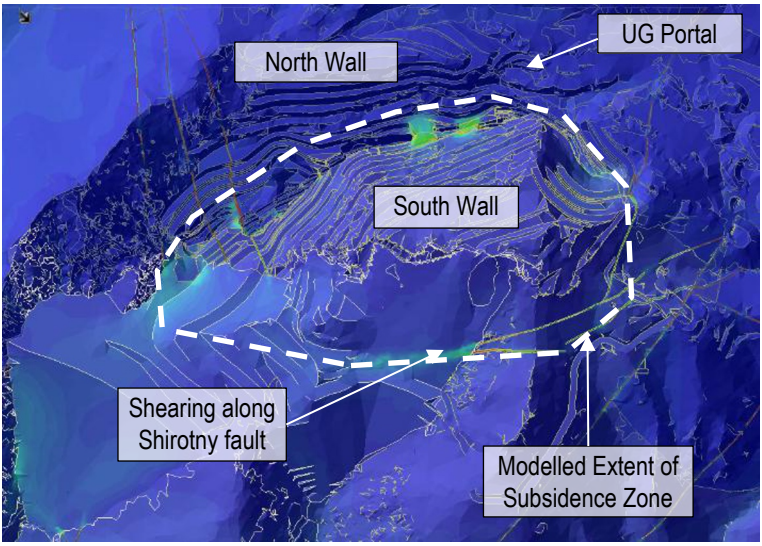

Figure 17. 3D FEM results showing Maximum Shear Strain. Plan view showing the modelled limit of the subsidence zone bounded by the Shirotny fault on the southern end.

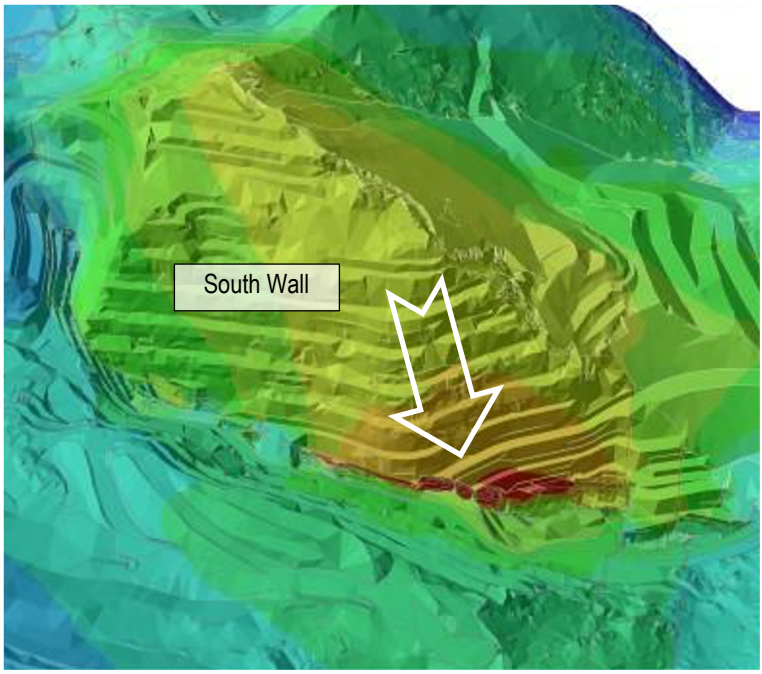

Figure 18. 3D FEM results showing modelled displacements on the south wall bounded by N-S striking faults with movement down toward the cave.

9 Discussion and Conclusions

The initial geotechnical investigations, model and stress-strain analysis provided valuable insights into expected ground behavior for the SLC excavations and subsidence zone.

Ground support requirements in various parts of the mine are expected to significantly increase over time in response to mining induced stresses. Further assessments of ground support design are also planned and include kinematic failure modes and dynamic loading.

The stress-strain modelling has many limitations and requires validation (and future updating) with a combination of further site investigations and the routine mapping and evaluation of rock mass quality and rock mass damage.

Monitoring systems are also required to validate the overbreak in the hanging wall, subsidence zone extents, and as well as rock burst risk.

Planned monitoring systems include prism monitoring and aerial photogrammetry for surface displacements and SLC material flow balances. Subsurface monitoring will include time domain reflectometry (TDR) for the hanging wall and micro-seismic monitoring. A trigger-action-response-plan (TARP) will be developed for managing subsidence and seismicity risks.

References

1. Nikonorov, V.V.: Ore deposits of Kyrgyzstan. Bishkek, 482p (2009).
2. Pak, N.T., Alpiev, M., Alpiev, Y.: Silver Mineralization at the Skarn Field Bozymchak (Kyrgyzstan). KRSU Bulletin 22(12), 173-181 (2022).
3. Avdeev, A.N., Zoteev, O.V., Sosnovskaya, E.L.: Geomechanical situation prediction in transition from open to underground mining of steeply dipping ore body by systems with caving. Mining Informational and Analytical Bulletin 5(2), 6-15 (2021).
4. Campbell, A.D.: A global review of recovery, dilution and draw control in sublevel caving mines. Proceedings of Caving 2022, 30 August – 1 September 2022, Adelaide, Australia, pp. 909-926 (2022).
5. Abzalov, M., Djenchuraeva, R., Alpiev, Y., Abzalov, S.: The geology of the Bozymchak Cu-Au skarn deposit, Tien Shan belt, Central Asia: emphasis on the geochemical characteristics of the granitoids. Applied Earth Science 128(3), pp. 106-123 (2019).
6. Zu, B., Seltmann, R., Xue, C., Wang, T., Dolgopolova, A., Li, C., Zhou, L., Pak, N., Ivleva, E., Chai, M., Zhao, X.: Multiple episodes of Late Paleozoic Cu-Au mineralization in the Chatkal-Kurama terrane: New constraints from the Kuru-Tegerek and Bozymchak skarn deposits, Kyrgyzstan. Ore Geology Reviews 111: 103077 (2019).
7. Alpiev, Y., Shamsutdinov, M.M., Akmatalieva, M.S. Geological Features and Physical and Mechanical Properties of the Bozymchak Deposit. KRSU Bulletin 23(4), pp. 162-168 (2023).
8. Alparov, A.: An Automated System for Monitoring Open Pit Walls taking into account Climate Properties. XII Annual International Conference on Modern Equipment and Technologies in Scientific Research, Russian Academy of Sciences in Bishkek, 22-24 April 2020, Bishkek, Kyrgyzstan, pp. 4-10 (2020).
9. Alpiev, Y., Shamsutdinov, M.M., Akmatalieva, M.S.: Geological Features and Physical and Mechanical Properties of the Bozymchak Deposit. KRSU Bulletin 23(4), pp. 162-168 (2023).
10. Deere, D.U.: Technical description of rock cores for engineering purposes. Felsmechanik und Ingenieurgeologie 1, pp. 16-22 (1963).
11. Bieniawski, Z.T.: Engineering Rock Mass Classifications. Wiley, New York, 251p (1989).
12. Barton, N., Lien, R., Lunde, J.: Engineering Classification of Rock Masses for the Design of Tunnel Support. Rock Mechanics 6, pp. 189-236 (1974).
13. Grimstad, E., Barton, N.: Updating of the Q-System for NMT. Proceedings of the International Symposium on Sprayed Concrete, 22-26 October 1993, Fagernes, pp. 46-66 (1993).
14. Barton, N.: Some new Q-value correlations to assist in site characterization and tunnel design. Int. J. Rock Mechanics & Mining Sciences 39, pp. 185-216 (2002).
15. Hoek, E., Brown, E.T.: The Hoek–Brown failure criterion and GSI – 2018 edition. J. Rock Mechanics & Geotechnical Engineering 11(3), pp. 445-463 (2019).
16. Hoek, E., Brown, E.T.: Underground Excavations in Rock. CRC Press, London, 536p (1980).
17. Martin, C.D., Kaiser, P.K., McCreath, D.R.: Empirical estimation of rock mass modulus. Int. J. Rock Mechanics & Mining Sciences 43, pp. 203-215 (1998).
18. Askaripour, M., Saeidi, A., Rouleau, A., Mercier-Langevin, P.: Rockburst in underground excavations: A review of mechanism, classification, and prediction methods. Underground Space 7, pp. 577-607 (2002).
19. Castro, L.A.M., Bewick, R.P., Carter, T.: An overview of numerical modelling applied to deep mining. In book: Innovative Numerical Modelling in Geomechanics, CRC Press, 22p. (2012).

20. Hedley, D.G.F.: Rockburst Handbook for Ontario Hardrock Mines. Energy, Mine and Resources, Ottawa, Canada (1992).
21. Stacey, T.R., Page, C.H.: Practical Handbook for Underground Rock Mechanics. Trans Tech Publications, Johannesburg, 78p (1988).
22. Jacobsson, L., Töyrä, J., Woldemedhin, B. & Krekula, H.: Rock support in the Kiirunavaara Mine. Proceedings of Ground Support 2013, 13-15 May 2013, Perth, Australia, pp. 401-410 (2013).
23. Norwegian Geotechnical Institute.: Handbook Using the Q-system Rock mass classification and support design. June 2022, Oslo, Norway, 56p (2022).